THE SEISMOLOGICAL SOCIETY OF AMERICA
400 Evelyn Ave., Suite 201
Albany, CA 94706-1375
(510) 525-5474; FAX (510) 525-7204
www.seismosoc.org

Bulletin of the Seismological Society of America, Vol. 104, No. 5, pp. 2240–2252, October 2014, doi: 10.1785/0120140022

A Study of the Sensitivity of Response Spectral Amplitudes on Seismological Parameters Using Algorithmic Differentiation

by Christian Molkenthin, Frank Scherbaum, Andreas Griewank, Nicolas Kuehn, and Peter Stafford

Abstract Response spectra are of fundamental importance in earthquake engineering and represent a standard measure in seismic design for the assessment of structural performance. However, unlike Fourier spectral amplitudes, the relationship of response spectral amplitudes to seismological source, path, and site characteristics is not immediately obvious and might even be considered counterintuitive for high oscillator frequencies. The understanding of this relationship is nevertheless important for seismic-hazard analysis. The purpose of the present study is to comprehensively characterize the variation of response spectral amplitudes due to perturbations of the causative seismological parameters. This is done by calculating the absolute parameter sensitivities (sensitivity coefficients) defined as the partial derivatives of the model output with respect to its input parameters. To derive sensitivities, we apply algorithmic differentiation (AD). This powerful approach is extensively used for sensitivity analysis of complex models in meteorology or aerodynamics. To the best of our knowledge, AD has not been explored yet in the seismic-hazard context. Within the present study, AD was successfully implemented for a proven and extensively applied simulation program for response spectra (Stochastic Method SIMulation [SMSIM]) using the TAPENADE AD tool. We assess the effects and importance of input parameter perturbations on the shape of response spectra for different regional stochastic models in a quantitative way. Additionally, we perform sensitivity analysis regarding adjustment issues of ground-motion prediction equations.

Introduction

The prediction of the expected ground motion for a given earthquake scenario (distance R, magnitude M_w, …) at a site of interest and the estimation of the maximum response of a structure to that input ground motion are of fundamental interest in earthquake engineering and seismic-hazard analysis. In this context, a response spectrum is a widely accepted measure for the severity of strong ground motion as it provides information about the response of structural or geotechnical systems to the imposed seismic loads. However, the relationship of response spectral amplitudes to seismological source, path, and site characteristics is, in contrast to Fourier spectral amplitudes, not immediately obvious and might even be considered counterintuitive for high oscillator frequencies. The quantitative dependence of response spectral amplitudes on seismological parameters that are known to influence ground motion is not well investigated. Its understanding is nevertheless important for seismic-hazard analysis, and the development of a complete understanding of this relationship still poses a significant challenge.

There are mainly two approaches that are currently employed to model high-frequency ground motions (greater than a few hertz) in the seismic-hazard context: (1) empirical prediction models or (2) ground-motion simulations such as those using the stochastic point source approach.

In the first approach, ground-motion prediction equations (GMPEs) are derived empirically through regression analysis on strong ground motion data sets. These prediction models give reliable estimates of the distribution of response spectral amplitudes if strong-motion data are abundant, assuming that future events will behave like those of the past. Empirical ground-motion relations are based only on a few input parameters and give an estimate of the ground-motion variability, which makes them very attractive for probabilistic seismic-hazard analysis (PSHA). However, not all of the model coefficients have a clear physical meaning, making it difficult to relate them to the underlying physical processes. Strictly speaking, one should expect GMPEs to be reliable only for the physical setting represented by the database used to derive them. As a consequence, this often prohibits the extrapolation or adjustment of the equation to a different region. Hence, a simple scaling of one GMPE to render it relevant for application in a different seismological environment

is not easily performed. In such cases, stochastic ground-motion models are often employed, which in theory allow ground-motion predictions to be made for a broad range of scenarios and have been found to be reliable in simulating ground motions of engineering interest (see table 5 in Boore, 2003; Atkinson and Boore, 2006; Edwards and Fah, 2013). The stochastic simulation technique (Boore, 2003) uses a seismological model to characterize the mean Fourier amplitude spectrum (FAS) of the strong motion affecting the site. In turn, the response spectral amplitudes can be directly estimated from the underlying FAS model of the ground motion using random vibration theory (RVT; Boore, 1983, 2003). The FAS model is based on the physics of the earthquake process and wave propagation, and it can inherently account for regional differences in the seismological attributes.

Indeed, strong-motion data are often scarce in many parts of the world and might not be sufficient for the development of reliable indigenous GMPEs. Campbell (2003) proposed an approach that employs GMPEs from other regions for performing seismic-hazard analysis. The selection and the adjustment of such imported or host GMPEs to a target region is a major challenge, because it needs to consider the regional differences in seismological characteristics like source, path, and site effects. Campbell's hybrid empirical method uses adjustment factors derived through stochastic ground-motion simulations for this purpose.

One could further improve the efficiency and accuracy of ground-motion scaling and adjustment of GMPEs if the sensitivity of the stochastic ground-motion simulations with respect to seismological attributes was known. Work along this line has been previously pursued in Douglas and Jousset (2011), in which sensitivity information revealed helpful insights for the development of GMPEs.

In addition, the accurate prediction of ground motion is a key component in PSHA (e.g., Bommer and Abrahamson, 2006). For low exceedance rates, the epistemic uncertainties of overall hazard are dominated by uncertainties regarding the ground-motion modeling (Toro, 2006). Hence, if a stochastic model is employed, uncertainties in the seismological parameters will directly map into uncertainties in the hazard results. Therefore, it is important to understand the effect that small perturbations of these parameters will have on the response spectrum and thus ultimately on the hazard. However, even though the stochastic ground-motion simulation technique is based on a relatively simple seismological model of the FAS, the mapping of perturbed seismological parameters into variations of response spectral amplitudes through the RVT framework is not easily accessible nor simply answered. Basically, RVT is a nonlinear mapping from the FAS to the response spectrum, which makes it difficult to assess the sensitivity of the latter to small perturbations in seismological parameters.

One way to perform sensitivity analysis for the response spectrum with respect to the seismological parameters is to calculate first-order derivatives, which may serve as a proxy for local differences in the output when there are small changes in the input. However, deriving exact partial derivatives of complex models for a differential sensitivity analysis (DSA) can be very difficult. Differentiating symbolically or by hand is often not possible, and although computing the derivatives by finite differences (FDs) may be easy to implement, the approach is plagued by drawbacks such as the step-size dilemma (round-off error, truncation error). Furthermore, to apply FD is computationally expensive or not even feasible if the output depends on a large number of input parameters.

To overcome these problems, we propose in this study to apply algorithmic differentiation (AD; Griewank and Walther, 2008). This extremely powerful approach is extensively used in sensitivity analysis of complex models, such as those used in meteorology (Marotzke and Giering, 1999) or in the field of aerodynamics (Gauger *et al.*, 2008). Sambridge *et al.* (2007) was the very first application of AD in geophysics. To the best of our knowledge, AD has not been explored yet in the context of seismic-hazard analysis. Given a computer implementation of a model, AD makes it possible, through a source code transformation, to obtain exact quantitative estimates of first-order sensitivities. The analysis and transformation of the computer code is done by a compiler-like AD tool (source-to-source code translator). As a result, one obtains a second computer code that evaluates the desired derivative information and the model output. This makes AD both theoretically and practically an invaluable tool. Considering a scalar model output (as in this study), AD directly delivers the sensitivities with respect to all of the input parameters in a very efficient way, independently of the number of input parameters.

The efficient calculation of sensitivities using AD represents a significant advantage over approaches based upon Monte-Carlo (MC) simulation. Because of the curse of dimensionality, MC simulations have the drawback of being computationally expensive if the number of inputs is high. The efficiency issue is even more important for highly complex models, for which a simulation is computationally very costly and, therefore, the calculation of sensitivities via MC simulations can become computationally infeasible. However, AD is only one way to study effects of parametric changes. For example, in contrast to AD, MC simulation does not require differentiability of the model and is able to assess global sensitivities.

The purpose of the present study is the quantitative characterization of response spectral amplitude variations simulated by a stochastic ground-motion model, due to perturbations in seismological parameters. We carry out a sensitivity analysis for the well known and extensively applied stochastic ground-motion simulation program called Stochastic Method SIMulation (SMSIM; Boore, 2003). This is done using a source code transforming AD tool. Absolute and normalized sensitivity coefficients for different seismological parameters and for different regional models are derived. Furthermore, we perform a sensitivity analysis regarding adjustment issues of GMPEs.

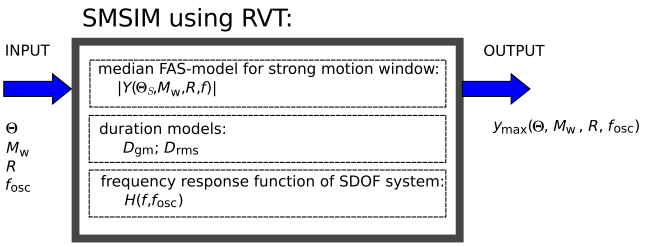

Figure 1. Sketch of stochastic ground-motion simulation model SMSIM. The color version of this figure is available only in the electronic edition.

Stochastic Ground-Motion Simulation

Response spectral amplitudes $y_{\max}$, defined as the maximum response of a single-degree-of-freedom (SDOF) system due to strong ground motion, can be simulated using the stochastic method. For this study, we adopt the well-known ground-motion simulation program SMSIM to estimate the response spectral amplitudes.

The stochastic spectrum simulation method has been extensively used in a broad range of applications in different tectonic regions and for a large range of magnitudes to predict response spectra (ground motions) worldwide as summarized, for example, in Silva *et al.* (1997) and Boore (2003). The simulation method is simple and has been proven to be reliable as its results are in close agreement with observations (Boore, 2003). The simulation technique has been developed over decades, and the version we describe here is based on RVT. We will give only a brief overview, a more thorough description of the method and the theory behind it can be found elsewhere (Rice, 1944; Cartwright and Longuet-Higgins, 1956; Boore, 1983, 2003).

The stochastic method assumes that high-frequency far-field ground motions (e.g., *S*-wave motions) of an earthquake scenario of magnitude M_{w} and hypocentral distance R can be described and modeled as a stationary bandlimited Gaussian noise of finite duration. Given the FAS of this stochastic process and its duration, response spectral amplitudes can be directly obtained using RVT. Therefore, SMSIM consists of three main components: (1) a model for the FAS of the strong motion (the stochastic model) ($|Y(\boldsymbol{\Theta}_S, M_{\mathrm{w}}, R, f|$), (2) duration models estimating the ground-motion duration (D_{gm}) and the duration used to compute the root mean square (rms) of the oscillator response (D_{rms}), and (3) the frequency response function of the SDOF system $H(f, f_{\mathrm{osc}})$ (Fig. 1). In the FAS model, the vector $\boldsymbol{\Theta}_S$ represents the set of seismological parameters defining the source, path, and site characteristics of the ground-motion generation process, for example, $\boldsymbol{\Theta}_S =$ (stress parameter, quality factor, geometrical spreading, kappa, …). The natural frequency of the SDOF oscillator is denoted by f_{osc}, and f represents a frequency of the input ground motion.

The peak amplitude of the SDOF oscillator response in the time domain $y_{\max}$ can be estimated using RVT as follows:

$$y_{\max}(\boldsymbol{\Theta}, M_{\mathrm{w}}, R, f_{\mathrm{osc}}) = \gamma(\boldsymbol{\Theta}, M_{\mathrm{w}}, R, f_{\mathrm{osc}}) \times y_{\mathrm{rms}}(\boldsymbol{\Theta}, M_{\mathrm{w}}, R, f_{\mathrm{osc}}), \quad (1)$$

in which y_{rms} is the rms response and γ represents the peak factor relating $y_{\max}$ to y_{rms}. The vector $\boldsymbol{\Theta}$ includes all parameters of the model, that is, the seismological parameters $\boldsymbol{\Theta}_S$ that define the FAS model as well as any additional parameters needed for the duration models. The peak factor γ as defined by Boore (2003) is as follows:

$$\gamma = \sqrt{2}\int_0^{\infty} 1 - \left[1 - \frac{m_2}{\sqrt{m_0 m_4}} e^{(-z^2)}\right]^{\left(\frac{1}{\pi}\sqrt{\frac{m_4}{m_2}} D_{\mathrm{gm}}\right)} \mathrm{d}z \quad (2)$$

and y_{rms} is modeled as:

$$y_{\mathrm{rms}} = \sqrt{\frac{m_0}{D_{\mathrm{rms}}}}, \quad (3)$$

in which m_k in both equations stands for the kth spectral moment:

$$m_k(\boldsymbol{\Theta}_S, M_{\mathrm{w}}, R, f_{\mathrm{osc}}) = 2\int_0^{\infty} (2\pi f)^k |Y(\boldsymbol{\Theta}_S, M_{\mathrm{w}}, R, f)|^2 \times |H(f, f_{\mathrm{osc}})|^2 \mathrm{d}f. \quad (4)$$

The core of the method is the seismological FAS model that is used to define the spectral moments (equation 4). From a physical point of view, the FAS describes the radiated source spectrum and its amplitude changes in the frequency domain due to wave propagation from the source to the site of interest. Thus, the FAS model considers source, path, and site attributes of the earthquake process. The underlying bandlimited mean FAS, $|Y(\boldsymbol{\Theta}_S, M_{\mathrm{w}}, R, f)|$, for a point source can be modeled in the following form as a sequence of filters:

$$|Y(\boldsymbol{\Theta}_S, M_{\mathrm{w}}, R, f)| = E(\boldsymbol{\Theta}_E, M_{\mathrm{w}}, f) \times P(\boldsymbol{\Theta}_P, R, f) \times G(\boldsymbol{\Theta}_G, f) \times I(f), \quad (5)$$

in which $E(\boldsymbol{\Theta}_E, M_{\mathrm{w}}, f)$ represents the source, $P(\boldsymbol{\Theta}_P, R, f)$ the path, and $G(\boldsymbol{\Theta}_G, f)$ the site contribution. The final filter, $I(f)$, accounts for the type of ground motion or response being simulated. For example, for the simulation of acceleration spectral ordinates $I(f) = (2\pi f)^2$. The seismological parameterization of source, path, and site properties is represented by the vectors $\boldsymbol{\Theta}_E$, $\boldsymbol{\Theta}_P$, $\boldsymbol{\Theta}_G$, respectively, in which $\boldsymbol{\Theta}_S = (\boldsymbol{\Theta}_E, \boldsymbol{\Theta}_P, \boldsymbol{\Theta}_G)$. In the present study, the radiated point-source spectrum $E(\boldsymbol{\Theta}_E, M_{\mathrm{w}}, f)$ is defined using Brune's single-corner ω-square model with constant stress parameter (Brune, 1970, 1971):

$$E(\boldsymbol{\Theta}_E, M_{\mathrm{w}}, f) = \frac{CM_0}{1 + (\frac{f}{f_c})^2}, \quad (6)$$

in which M_0 is the seismic moment that has units of dyn·cm (when the coefficients of the following two equations are adopted) and is related to the moment magnitude M_{w} as follows (Hanks and Kanamori, 1979):

$$M_w = \frac{2}{3}\log_{10} M_0 - 10.7. \quad (7)$$

The corner-frequency f_c of Brune's source spectrum in hertz is given by

$$f_c = 4.9 \times 10^6 \beta_S (\Delta\sigma / M_0)^{1/3}, \quad (8)$$

in which $\Delta\sigma$ is the stress parameter in units of bar, and β_S is the shear-wave velocity in the vicinity of the earthquake source given in kilometers per second. The constant scaling factor C introduced in equation (6) is defined as

$$C = \frac{\langle R_{\Theta\Phi}\rangle V F}{4\pi\rho_S \beta_S^3 R_0}, \quad (9)$$

in which $\langle R_{\Theta\Phi}\rangle$ represents the average radiation pattern for far-field shear waves ($\langle R_{\Theta\Phi}\rangle = 0.55$), V is the partition of total shear-wave energy into horizontal components ($V = 1/\sqrt{2}$), F represents the effect of the free surface ($F = 2$) whereas ρ_S and β_S are the density and shear-wave velocity of the source location, respectively, and R_0 is a reference distance for geometrical spreading (usually $R_0 = 1$ km).

The loss of energy due to the simplified path effect $P(\boldsymbol{\Theta}_P, R, f)$ of the wave propagation through a geological medium is modeled as a product of geometrical spreading (simplified here as $1/R^\eta$) and a crustal damping function:

$$P(\boldsymbol{\Theta}_P, R, f) = \frac{1}{R^\eta} \exp\left[-\frac{\pi f R}{Q_0 f^\alpha c_q}\right], \quad (10)$$

in which the regional quality factor $Q(f) = Q_0 f^\alpha$ accounts for anelastic attenuation and wave energy loss due to scattering in the crust, and c_q is the shear-wave phase velocity used in the determination of $Q(f)$.

The site effects are modeled by

$$G(\boldsymbol{\Theta}_G, f) = A(f) \exp[-\pi f \kappa_0], \quad (11)$$

in which the exponential expression ($e^{-\pi f \kappa_0}$) represents the kappa filter introduced by Anderson and Hough (1984). This filter describes the distance-independent high-frequency decay of the spectrum due to near-surface attenuation. The frequency-dependent site-specific amplification due to the vertical velocity gradient in the crust $A(f)$ can be modeled using a generic rock site frequency-response function as $\hat{A}(V_{S30}, f)$, with V_{S30} (the time-averaged shear-wave velocity of the upper 30 m of geomaterial) as the main controlling parameter. In this study, $\hat{A}(V_{S30}, f)$ is constructed in such a way that for $V_{S30} = 620$ m/s and $V_{S30} = 2800$ m/s it converges to the western and eastern United States generic rock models, respectively, of Boore and Joyner (1997). For each V_{S30} in that range, $\hat{A}(V_{S30}, f)$ is interpolated between these limiting cases. For details of the derivation, see Cotton *et al.* (2006). This model is restricted to generic rock sites with V_{S30} values greater than 620 m/s, consequently soil sites are not considered.

Besides the description of the Fourier spectrum, the duration models for D_{gm} and D_{rms} are important components of the method; see equations (2), (3), and Figure 1. According to Boore (2003), the ground-motion duration (D_{gm}) is modeled as the sum of source duration, which is inversely related to the source corner frequency f_c, and path duration as follows:

$$D_{gm}(M_w, \Delta\sigma, \beta_S, \tau, R) = \frac{1}{f_c(M_w, \Delta\sigma, \beta_S)} + \tau R, \quad (12)$$

in which the parameter τ controls the path-dependent duration, R represents the source-to-site distance in kilometers, and the magnitude M_w and the stress parameter $\Delta\sigma$ define the source corner frequency f_c (equation 8). D_{rms} can be modeled in different ways (see Boore and Joyner, 1984; Liu and Pezeshk, 1999; Boore and Thompson, 2012). In this study, D_{rms} is set to D_{gm} for simplicity.

The absolute value of the frequency response function of an SDOF oscillator used to derive pseudospectral acceleration from an FAS of acceleration is given by

$$|H(f, f_{osc})| = \frac{f_{osc}^2}{\sqrt{(f^2 - f_{osc}^2)^2 + (2 f f_{osc}\zeta)^2}}, \quad (13)$$

in which ζ represents the damping ratio of the SDOF system.

Algorithmic Differentiation and Sensitivity Analysis

Algorithmic differentiation is a powerful tool for performing DSA of the model behavior due to (slight) parameter variations. Sensitivities measure how much a slight change in the input parameters changes the model output. Appreciating the robustness of a model involves identifying the highly sensitive parameters. Furthermore, derivative information procured with AD can be used with numerical optimization algorithms for estimating model parameters given a set of observed data. To quantify the impact of slight seismological parameter variations on response spectral amplitudes, we differentiate the stochastic ground-motion simulation program SMSIM using AD. Evaluating the differentiated program enables the derivation of sensitivities for a DSA in a very efficient way.

Broadly speaking, the key question in DSA is how the output of a given response function (or model), $f(\boldsymbol{x})$, with input $\boldsymbol{x}$, varies with respect to a given slight change in the model inputs $\delta\boldsymbol{x}$. For simplicity, we assume a scalar model output. Mathematically, parameter sensitivities or local, first-order sensitivity coefficients S_i are defined as the partial derivatives of the model output $f(\boldsymbol{x})$ with respect to its input parameters x_i as follows:

$$S_i = \left.\frac{\partial f(\boldsymbol{x})}{\partial x_i}\right|_{\boldsymbol{x}_0}. \quad (14)$$

This estimated local behavior of the model corresponds to a linear approximation as a first-order Taylor expansion at the reference point $\boldsymbol{x}_0$ and is generally not valid for parameter ranges far from $\boldsymbol{x}_0$. We assert, therefore, that in this context DSA is a method for assessing local sensitivities.

Deriving absolute sensitivities S_i allows one to assess the impact of perturbations of the individual parameters on the response. Furthermore, S_i can be directly used for model fitting (inversion) purposes or for first-order uncertainty analysis. However, physical input parameters are generally not directly comparable with each other, either because they are expressed in different scales or units or because they express different physical quantities. Thus, comparing absolute sensitivities for an importance analysis of the inputs might be difficult to understand and may possibly be misleading. To remove these effects in problematic cases, it is advisable to calculate the so-called relative (logarithmic) sensitivities Φ_i. These are absolute sensitivities S_i normalized by $x_{i,0}/y_0$ defined as follows (Frank, 1978; Saltelli, 2000):

$$\Phi_i = S_i \times \frac{x_{i,0}}{y_0} \approx \frac{\Delta y}{y_0}\left(\frac{\Delta x_i}{x_{i0}}\right)^{-1}, \tag{15}$$

in which S_i stands for the absolute sensitivity with respect to the input parameter x_i, y_0 is the model output ($y_0 = f(\boldsymbol{x}_0)$) evaluated at the reference point $\boldsymbol{x}_0$, and $x_{i,0}$ is the ith component of $\boldsymbol{x}_0$. In this way, a fractional or percentage change $\Delta x_i/x_{i,0}$ of the input parameter (as fixed fraction of its base value) is related to the fractional or percentage change of the output $\Delta y/y_0$. For the Φ_i to be defined, the model output y_0 must be nonzero, which is the case in our study. There is no silver bullet, however, for representing sensitivities. Indeed, there exist several ways to scale absolute sensitivities including a normalization to the standard deviation or to the range of the inputs (Morgan, 1990; Helton, 1993; Saltelli, 2000). In this study, absolute sensitivities are not normalized to the range or to the variation of the inputs as the obtained derivatives are local estimates. Moreover, the considered regional stochastic models are themselves point estimates.

The partial derivatives (equation 14) can be calculated by AD, which has been proven to be an extremely powerful tool for this purpose, enabling very efficient evaluation with machine accuracy (Griewank *et al.*, 2012). The method has been extensively applied for evaluating sensitivities to perturbations in independent variables of complex models, for example, empirical parameters, boundary, or initial condition problems (Marotzke and Giering, 1999). AD is a chain rule-based method and has the enormous advantage that it can be applied directly on existing computer code for a model independent of its complexity, at least in principle. Moreover, AD does not suffer from accuracy drawbacks nor does it have additional increment parameters found in FD techniques. Because of the associativity of the chain rule of differentiation, derivatives can be propagated either in forward direction together with the function evaluation (from the inputs to the outputs) or in reverse direction after the function was evaluated (from the output to the inputs). Thus, two fundamental modes of AD exist: the forward mode constructing the tangent-linear model (TLM) and the reverse mode constructing the adjoint model (ADM).

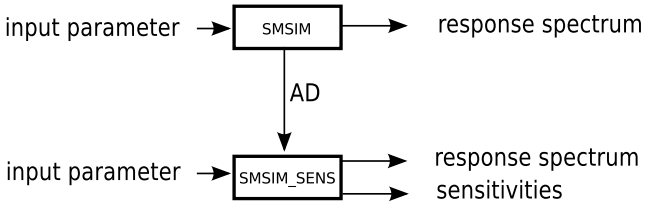

Figure 2. Algorithmic differentiation (AD) sketch for SMSIM.

Generically speaking, AD differentiates programs. The original program, here SMSIM, is transformed into a new program, SMSIM_SENS, which computes not only the model output but also the required derivative values (sensitivities) in floating point arithmetic (Fig. 2). Differentiation of the program can take place as either source code transformation or via operator overloading. Doing this manually is very time consuming, tedious, and error prone. However, over the past decades, several mature AD tools have been developed that can be applied to complex models built with elaborate source code (e.g., ≥100,000 lines of FORTRAN code). Below, we give a brief introduction into AD, and for a more detailed view, we recommend that the interested reader consults Griewank and Walther (2008).

The basic assumption behind AD is that every computer program can be seen as the composition of elementary functions φ_i, composed either of a set of intrinsic functions (e.g., sin, cos, exp), arithmetic operations (e.g., $+$, $-$, $\times$, $/$), or a combination of these, that deliver intermediate numerical values v_i. Following the notation of Griewank and Walther (2008), a program is a composite function $\boldsymbol{y} = f(\boldsymbol{x})$ with $f{:}\mathbb{R}^n \rightarrow \mathbb{R}^m$ that involves $n + l$ intermediate values v_i and consists of three parts: initialization, evaluation, and extraction, as given in Table 1. The second column of Table 1 shows the general formalization of a function evaluation on a computer. To illustrate this formalism in an easy way, we also show a corresponding evaluation procedure (i.e., list of elementary calculations) for a simple example ($y = x_1 \times \sin(x_1 + x_2)$) in the third column. The initialization part copies the inputs (i.e., independent variables) to internal variables (v_{-1}, v_0). The actual calculation is performed in the evaluation part (v_1, v_2, v_3). The last part (extraction) copies the resulting values to the output (i.e., dependent variables). In the example, a single scalar-valued output is considered ($y_1 = v_3$). The symbol $j \prec i$ denotes that v_i depends directly on v_j, in which v_j is a predecessor of v_i and enters directly into the calculation of v_i, such that $\partial\varphi_i/\partial v_j \neq 0$. The evaluation of each elemental function φ_i results in a corresponding intermediate value v_i. The n-independent inputs x_i, initialized in the first loop, are mapped onto m-dependent outputs y_k, extracted in the last part. The extraction simply means the copy of the last intermediate values to the output of the function. For the differentiation, AD

Table 1

General Evaluation Procedure of Computer Code for a Function $f:\mathbb{R}^n \to \mathbb{R}^m$ Illustrated by an Example of a Simple Function Evaluation of Expression $y = x_1 \sin(x_1 + x_2)$

Part	General Form	Example
	$f:\mathbb{R}^n \to \mathbb{R}^m$	$f:\mathbb{R}^2 \to \mathbb{R}$
	$\boldsymbol{y} = f(\boldsymbol{x})$	$y = x_1 \sin(x_1 + x_2)$
Initialization	for $i = 1, \ldots, n$	
	$v_{i-n} = x_i$	$v_{-1} = x_1$
		$v_0 = x_2$
Evaluation	for $i = 1, \ldots, l$	
	$v_i = \varphi_i(v_j)_{j \prec i}$	$v_1 = \varphi_1(v_{-1}, v_0) = v_{-1} + v_0$
		$v_2 = \varphi_2(v_1) \quad = \sin(v_1)$
		$v_3 = \varphi_3(v_{-1}, v_2) = v_{-1} v_2$
Extraction	for $i = m - 1, \ldots, 0$	
	$y_{m-i} = v_{l-i}$	$y_1 = v_3$

simply applies the chain rule to the composition of φ_i. To that end, the rules of differential calculus for arithmetic operations (e.g., product rule,…) and a library of derivatives for the intrinsic functions (symbolic differentiation) are used.

In the forward mode, the original program code is augmented by statements for the evaluation of the derivative values $\dot{v}_i$ for each intermediate v_i. The derivative values $\dot{v}_i$ are accumulated in the forward direction simultaneously with the intermediate values v_i (from the inputs to the outputs). The generated code is called TLM. The corresponding TLMs to the evaluation procedures given in Table 1 are listed in Table 2 (for a general case and for a simple example). Similar to Table 1, the initialization part copies the inputs to internal variables (v_{-1}, v_0, $\dot{v}_{-1}$, $\dot{v}_0$). There are additional inputs $\dot{x}_1$ and $\dot{x}_2$, which define the direction of the derivative. Before using the TLM, the direction of the partial derivative has to be selected by the initialization of the corresponding $\dot{x}_i$ to one while all other components of $\dot{\boldsymbol{x}}$ are set to zero (seeding). A single run of the TLM gives, in addition to the model outputs, the partial derivatives of all m outputs with respect to one input parameter, for example $\partial y_1/\partial x_1, \ldots, \partial y_m/\partial x_1$ in the case of x_1. This corresponds to a column of the Jacobian matrix supposing $f:\mathbb{R}^n \to \mathbb{R}^m$ or to a single entry of the gradient in the case of $f:\mathbb{R}^n \to \mathbb{R}$ (as in our case). In Table 2 (third column), to obtain $\partial y_1/\partial x_1$ one has to choose $\dot{x}_1 = 1$ and $\dot{x}_2 = 0$ (seeding). After a single run of TLM, $\partial y_1/\partial x_1$ is given by the third column last row ($(\partial y_1/\partial x_1) = \sin(x_1 + x_2) \times 1 + x_1 \cos(x_1 + x_2)(1 + 0)$). This procedure (seeding and a TLM run) has to be repeated for each input to get a complete gradient of a scalar model output. The computational cost for evaluating forward sensitivities by the TLM increases linearly with the number of inputs n (independent variables) and can become infeasible for very large n. Thus, the TLM approach is suitable for models with only a few inputs but with many outputs. The computational complexity is comparable with that of FD, but still the advantage of no loss of accuracy and no additional increment parameter remains.

However, using AD in the case of $m = 1$ (a model with a scalar-valued output $\boldsymbol{y} = f(\boldsymbol{x})$), the gradient can be obtained in a very efficient way using the reverse mode of AD. An ADM is constructed by applying the chain rule backward (from the output to the inputs). Each intermediate value v_i is associated with an adjoint variable $\bar{v}_i = \partial y/\partial v_i$ and by definition $\bar{y} = 1$. The adjoints will be propagated in the reverse direction through the evaluation procedure. This requires one to process the original code backward (program reversal) with the intermediates v_i in reverse order. Thus, the reverse mode of AD consists of two stages. The first stage derives and stores the intermediates v_i (forward sweep) as given in Table 1. It is essentially a copy of the original code. The second part evaluates the adjoints backward through the evaluation procedure (return sweep) using intermediates v_i, derived in the first part. The return sweep of the ADM corresponding to Table 1 is given in the nonincremental form in Table 3 (for a general case and for a simple example). The symbol $j \succ i$ denotes that v_j is a direct successor of v_i in the original code. Hence, one collects all contributions to the actual adjoint $\bar{v}_i$ by summing over all successors $j \succ i$. The partial derivatives of the scalar output with respect to all inputs are given directly by $\bar{v}_i$ for $i = n - 1, \ldots, 0$, shown in the last rows of Table 3 (extraction part).

The enormous advantage of the ADM for a scalar-valued output is that one run gives directly the model sensitivities (gradient) with respect to all inputs, independently of the number of inputs. The computational cost to evaluate the ADM is only a small factor higher (usually < 10) than the evaluation costs for the original model itself (Griewank and Walther, 2008; Naumann, 2012). This makes the adjoint mode of AD very appealing for the evaluation of the gradient for scalar-valued objective functions, which is the case in our study. The disadvantage of the reverse mode (ADM) is that it requires one to keep the intermediate variables v_i in storage, which can be challenging for highly complex models, but this is not the case for SMSIM.

Practical Implementation of AD for SMSIM

Powerful and mature AD tools for the differentiation of computer code (mainly for programs written in FORTRAN or C) are freely available. For the construction of the ADM for SMSIM, which is written in FORTRAN, we used the source code transforming AD tool TAPENADE (Hascoët and Pascual, 2004). It is a flexible and efficient AD tool for FORTRAN code, providing the means to apply both the forward and reverse modes.

Some minor code modifications were necessary to clarify the differential dependencies in the code. In addition, we had to substitute an ordinary differential equation (ODE) solver routine, which computes the spectral moments, as the embedded method proved unstable when combined with AD. The adaptive ODE solver was replaced by a numerical quadrature routine that made the ADM stable without sacrificing any accuracy in the spectral moment computation. Theoretically, the AD methodology interprets the actual evaluation process as a straight-line code with a finite and fixed number

Table 2
Formalized Forward Mode of AD (TLM) for the General Case and for the Simple Example of Table 1

Part	General form	Example	
	$f:\mathbb{R}^n \to \mathbb{R}^m$	$f:\mathbb{R}^2 \to \mathbb{R}$	
	$\boldsymbol{y} = f(\boldsymbol{x})$	$y = x_1 \sin(x_1 + x_2)$	
Initialization	for $i = 1, \ldots, n$		
	$v_{i-n} = x_i$	$v_{-1} = x_1$	
		$v_0 = x_2$	
	$\dot{v}_{i-n} = \dot{x}_i$	$\dot{v}_{-1} = \dot{x}_1$	
		$\dot{v}_0 = \dot{x}_2$	
Evaluation	for $i = 1, \ldots, l$		
	$v_i = \varphi_i(v_j)_{j \prec i}$	$v_1 = \varphi_1(v_{-1}, v_0)$	$= v_{-1} + v_0$
	$\dot{v}_i = \sum_{i:j \prec i} \frac{\partial}{\partial v_j} \varphi_i(v_j)_{j \prec i} \dot{v}_j$	$\dot{v}_1 = \frac{\partial \varphi_1(v_{-1}, v_0)}{\partial v_{-1}} \dot{v}_{-1} + \frac{\partial \varphi_1(v_{-1}, v_0)}{\partial v_0} \dot{v}_0$	$= \dot{v}_{-1} + \dot{v}_0$
		$v_2 = \varphi_2(v_1)$	$= \sin(v_1)$
		$\dot{v}_2 = \frac{\partial \varphi_2(v_1)}{\partial v_1} \dot{v}_1$	$= \cos(v_1)\dot{v}_1$
		$v_3 = \varphi_3(v_{-1}, v_2)$	$= v_{-1} v_2$
		$\dot{v}_3 = \frac{\partial \varphi_3(v_{-1}, v_2)}{\partial v_{-1}} \dot{v}_{-1} + \frac{\partial \varphi_3(v_{-1}, v_2)}{\partial v_2} \dot{v}_2$	$= v_2 \dot{v}_{-1} + v_{-1} \dot{v}_2$
Extraction	for $i = m - 1, \ldots, 0$		
	$y_{m-i} = v_{l-i}$	$y_1 = v_3$	
	$\dot{y}_{m-i} = \dot{v}_{l-i}$	$\dot{y}_1 = \dot{v}_3$	$= \sin(x_1 + x_2)\dot{x}_1 + x_1 \cos(x_1 + x_2)(\dot{x}_1 + \dot{x}_2)$

Table 3
Return Sweep of Reverse Mode (ADM) for a General Case and for the Simple Example of Table 1

Part	General form	Example	
Evaluation	$\bar{y}_1 = 1.0$	$\bar{y}_1 = 1.0$	
	$\bar{v}_l = \bar{y}_1$	$\bar{v}_3 = \frac{\partial y_1}{\partial v_3} = \bar{y}_1$	
	for $i = l - 1, \ldots, 1 - n$		
	$\bar{v}_i = \sum_{j:j \succ i} \bar{v}_j \frac{\partial}{\partial v_i} \varphi_j(v_i)_{i \prec j}$	$\bar{v}_2 = \frac{\partial y_1}{\partial v_2} = \bar{v}_3 \frac{\partial \varphi_3(v_{-1}, v_2)}{\partial v_2}$	$= \bar{v}_3 v_{-1}$
		$\bar{v}_1 = \frac{\partial y_1}{\partial v_1} = \bar{v}_2 \frac{\partial \varphi_2(v_1)}{\partial v_1}$	$= \bar{v}_2 \cos(v_1)$
		$\bar{v}_0 = \frac{\partial y_1}{\partial v_0} = \bar{v}_1 \frac{\partial \varphi_1(v_{-1}, v_0)}{\partial v_0}$	$= \bar{v}_1 \times 1$
		$\bar{v}_{-1} = \frac{\partial y_1}{\partial v_{-1}} = \bar{v}_1 \frac{\partial \varphi_1(v_{-1}, v_0)}{\partial v_{-1}} + \bar{v}_3 \frac{\partial \varphi_3(v_{-1}, v_2)}{\partial v_{-1}}$	$= \bar{v}_1 + \bar{v}_3 v_2$
Extraction	for $i = n, \ldots, 1$		
	$\bar{x}_i = \bar{v}_{i-n}$	$\bar{x}_2 = \frac{\partial y_1}{\partial x_2} = \bar{v}_0$	$= x_1 \cos(x_1 + x_2)$
		$\bar{x}_1 = \frac{\partial y_1}{\partial x_1} = \bar{v}_{-1}$	$= x_1 \cos(x_1 + x_2) + \sin(x_1 + x_2)$

of elementary instructions. Typically, real world codes incorporate program branches and other adaptive elements so that the input–output relation is only piecewise differentiable. Very often, the derivative of the smooth pieces still reflects quite well the sensitivities of the outputs with respect to the inputs. However, sometimes the computed derivative may be erratic and unusable, for example if an ODE is solved with strongly adaptive step size selection. Generally freezing grids during the evaluation of derivatives is likely to produce acceptable results. In our problem, numerical integration was performed using a quadrature algorithm with fixed abscissas and weights rather than an adaptive ODE solver.

In addition to the possibility of encountering stability issues such as that just mentioned, there are some additional practical limitations, or considerations, that relate to the use of AD. First, the complete source code for the simulation model must be available, preferably in one procedural language (e.g., FORTRAN or C). Second, as in the case of parallelizable data, dependencies should be recognizable to the AD tool. For example, indirect addressing into work arrays or inconsistent common block partitioning may degrade runtime performance and lead to excessive storage requirements, especially when run in reverse mode. Finally, taking liberties with the language standards may inhibit the AD tool from producing correct derivatives, even if the undifferentiated code executes correctly.

In the case of SMSIM, the source code to source code transformation using the AD tool TAPENADE worked without trouble, following the relatively minor code modification mentioned previously. The transformation of the enhanced

Table 4
Partial Derivative Values of the Model Output (Spectral Acceleration) with Respect to the Input $\Delta\sigma$ (Stress Parameter) for Different Oscillator Frequencies

Method*	Step Size	1 Hz	3 Hz	10 Hz	100 Hz
ADM	–	1.561843	3.883376	4.512044	1.775013
TLM	–	1.561843	3.883376	4.512044	1.775013
FD	1×10^{-01}	1.561524	3.882863	4.511507	1.774784
FD	1×10^{-03}	1.561839	3.883371	4.512039	1.775011
FD	1×10^{-05}	1.561843	3.883376	4.512044	1.775013
FD	1×10^{-07}	1.561840	3.883378	4.512043	1.775014
FD	1×10^{-09}	1.561801	3.883883	4.512231	1.775391
FD	1×10^{-11}	1.568878	3.944933	4.547474	1.807621
FD	1×10^{-13}	1.705303	4.547474	4.547474	3.126388

*ADM, adjoint model; TLM, tangent linear model; FD, finite differences.

source code by the AD tool is very fast and takes less than 10 s on a 2011 iMac with 8 GB of RAM and 2.5 GHz processor.

The accuracy of the derived ADM was validated by comparisons between the derivatives it produces and those obtained by (1) the TLM and (2) FDs with decreasing step size. The derivative values obtained by ADM and TLM are identical and coincide with those obtained by FD when an optimal step size is employed. Results of an example experiment proving the accuracy are given in Table 4. The input parameter values correspond to the regional parameterization of western North America (WNA) with a magnitude–distance scenario of M_w 6 and $R = 10$ km. As shown in Griewank *et al.* (2012), the forward and reverse modes are backward stable in that the numerically computed derivatives correspond to the exact values for a slightly perturbed evaluation procedure.

Application: Sensitivity of Response Spectral Amplitudes

In this section, we present the results of the sensitivity analyses that have been conducted using the derived ADM to study variations in the response spectral amplitudes due to slight changes in the seismological parameters.

Sensitivities of Different Regional Stochastic Models

First, we investigate the behavior of response spectral variations for two different regional stochastic models. For this purpose, we calculate the derivatives of the spectral acceleration with respect to the different seismological parameters using the ADM and assess their sensitivities according to equation (14). To facilitate simple comparisons with GMPEs, we consider $\ln(y_{max})$ as the model output. In addition, we derive the relative sensitivities of y_{max} according to equation (15). We use the parameters proposed by Campbell (2003) for WNA and eastern North America (ENA), because these models represent different tectonic units (active crustal and stable continental, respectively). From an AD viewpoint, there are approximately 15–20 inputs (i.e., independent variables) for these regional models, which map to a single scalar output (i.e., the dependent variable) for each considered oscillator frequency. However, note that the method can be applied to any regional model, including more complex stochastic models.

Table 5
Parametrization of ENA and WNA after Campbell (2003)

Parameter	WNA with Θ_{WNA}*	ENA with Θ_{ENA}†
Source spectrum	Brune ω-square, point source	Brune ω-square, point source
Stress parameter, $\Delta\sigma$ (bar)	100	150
Average radiation pattern, $\langle R_{\Theta\Phi} \rangle$	0.55	0.55
Partition of total shear-wave energy, V	$1/\sqrt{2}$	$1/\sqrt{2}$
Effect of the free surface, F	2	2
Geometrical spreading, η	$1/R^{\eta} = 1/R$	$1/R^{\eta} = 1/R$
Ground-motion duration, D_{gm} (s)	$1/f_c + 0.05R$	$1/f_c + 0.05R$
Rms duration, D_{rms} (s)	$D_{rms} = D_{gm}$	$D_{rms} = D_{gm}$
Path attenuation quality factor, Q	$180f^{0.45}$	$680f^{0.36}$
Shear velocity, β_S (km/s)	3.5	3.6
Density, ρ_S (g/cc)	2.8	2.8
Site attenuation, κ_0 (s)	0.04	0.006
Site amplification	Generic rock site $V_{S30} = 620$ m/s Quarter-wavelength approximation	Generic rock site $V_{S30} = 2800$ m/s Quarter-wavelength approximation

*Input parameters Θ_{WNA} for western North America
†Input parameters Θ_{ENA} for eastern North America

The different input parameters $\boldsymbol{\Theta}_S$ for the two models are summarized in Table 5. For simplicity, we use the same duration model for both the ground-motion durations D_{gm} and the rms duration D_{rms} (Table 5).

We calculate first-order absolute (S_i) and relative sensitivities (Φ_i) for response spectral amplitudes with respect to M_w, $\Delta\sigma$, Q_0, and κ_0. Results are shown in Figures 3 and 4 for different magnitudes (M_w 6 and 7) and distance scenarios ($R_{hypo} = 10$ km and 100 km). Figure 3 shows the change of the model output ($\ln y_{max}$) due to small absolute changes of the inputs. Considering y_{max} instead of $\ln y_{max}$, Figure 3 depicts the fractional change (relative error) of y_{max} due to an absolute change in the inputs. One can assess and compare the impact of each individual parameter on the output for the different scenarios or settings. However, one must take caution when making direct comparisons between the sensitivities for different parameters as these absolute sensitivities have different units and scales. Thus, to get a more complete picture, we also show relative sensitivities in Figure 4, which relates a percentage change of an input (relative error) to the percentage change of y_{max} (relative error of the output).

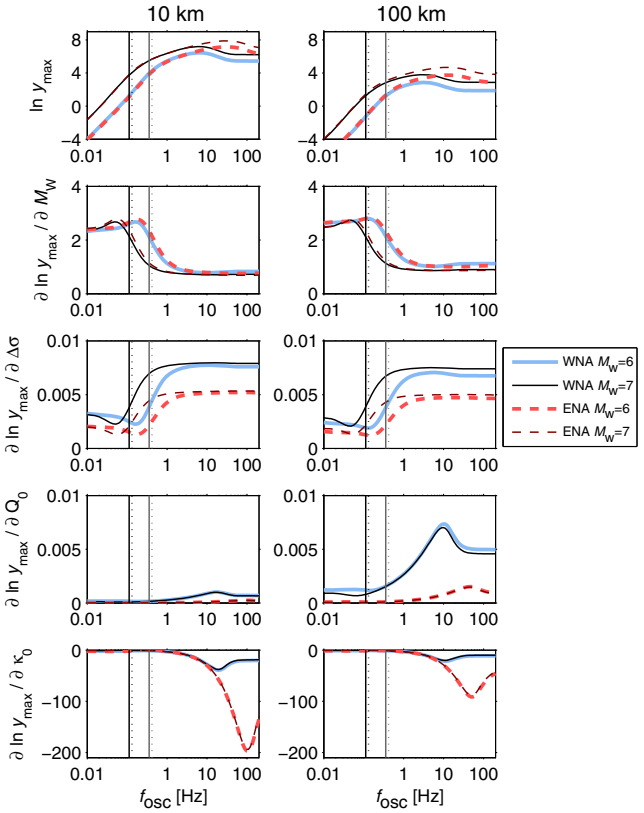

Figure 3. First row shows simulated response spectra for different magnitude–distance scenarios for ENA and WNA, respectively. Corresponding sensitivities with respect to magnitude (M_w), stress parameter ($\Delta\sigma$), Q_0, and κ_0 are shown in second to fifth rows. (Left) for 10 km and (right) for 100 km. The vertical lines indicate the source corner frequencies of the input ground-motion FAS (f_c), solid lines for WNA, and dotted for ENA, M_w 6 (light shade) and M_w 7 (dark shade). The color version of this figure is available only in the electronic edition.

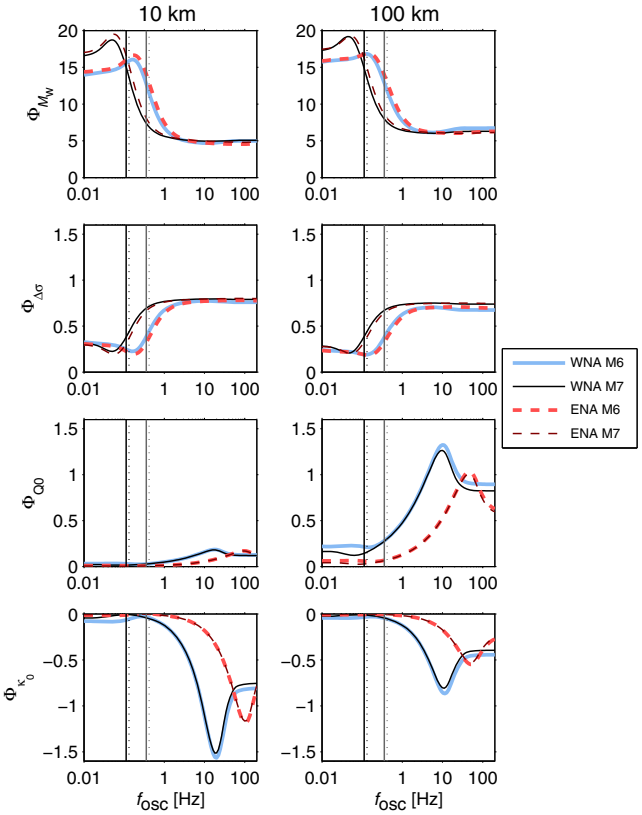

Figure 4. Relative sensitivities Φ_i of ENA and WNA with respect to magnitude (M_w, first row), stress parameter ($\Delta\sigma$, second row), Q_0 (third row), and κ_0 (fourth row). (Left) for 10 km and (right) for 100 km. The vertical lines indicate the position of source corner frequencies of the input ground motion (f_c), black for M_w 7 (solid, WNA; dotted, ENA) and similarly gray for M_w 6 (solid, WNA; dotted, ENA). The color version of this figure is available only in the electronic edition.

Positive/negative sensitivity values indicate increase/decrease of the model output due to a slightly increased input parameter value. The term small perturbation refers to a local change of an input $\delta\Theta_i$ for which the model behavior (change in the output) can be still approximated by a first-order Taylor expansion in an acceptable way (with an acceptable error). Accordingly, the magnitude of acceptable local changes in the inputs also depends on the reference point. For example, a rough approximation of upper bounds on small perturbations in the parameters $\Delta\sigma$, Q_0, and κ_0 that lead to an acceptable Taylor approximation for WNA and ENA is $\delta\Delta\sigma \approx 26$ (38) bar, $\delta Q_0 \approx 46$ (184), and $\delta\kappa_0 = 0.0033$ (0.00067) s (values for the ENA model are given in parenthesis). These values are proposed assuming that an error of $\leq 1.5\%$ of the surrogate model (Taylor expansion) is tolerable and are based on the consideration of a magnitude–distance scenario of $R_{hypo} = 10$ km and M_w 6.

One of the first trends to notice in Figure 3 is that for short distances and large magnitudes, slight changes in the parameter κ_0 cause large changes in the response spectral amplitudes for high oscillator frequencies. This is expected, as κ_0 controls the high-frequency attenuation of the input ground-motion FAS (Anderson and Hough, 1984). The impact of κ_0 becomes more significant with decreasing values of κ_0. For small values of κ_0, such as that commonly used for ENA ($\kappa_0 = 0.006$), only a small portion of the high-frequency input motion is filtered out at short distances, which leads to the large sensitivity to κ_0 for ENA. On the other hand, for the WNA model ($\kappa_0 = 0.04$) the sensitivity to κ_0 is much smaller because a larger amount of high-frequency input motion is already filtered out. Thus, slight absolute changes in κ_0 have a smaller effect on the response spectrum. However, the same slight relative error (relative change) in κ_0 cause a larger relative error (relative change) of y_{max} for the WNA model than for ENA for values of $f_{osc} < 50$ Hz (Fig. 4). The base values of κ_0, which are the reference for relative changes, are very different for WNA ($\kappa_0 = 0.04$) and ENA ($\kappa_0 = 0.006$). Consequently, the same considered relative change in κ_0 for both the models is equivalent to a much larger absolute change in κ_0 for the WNA model (factor >6.6) than for ENA. The sensitivity of the spectral acceleration to κ_0 decreases with

distance, which may be explained by the additional impact of path-introduced high-frequency attenuation. This effect also makes the estimation of κ_0 very hard if there is not enough station coverage near the source (Ktenidou *et al.*, 2014). At 100 km for example, the relative sensitivities for Q_0 are larger than those of κ_0 (Fig. 4). Furthermore, sensitivity functions with respect to κ_0 depend strongly on f_{osc} and are peaked for large f_{osc} (Figs. 3 and 4). Thus, slight changes in κ_0 strongly affect the response spectral shape at high f_{osc} and have a strong influence on the position of critical points like the maximum (f_{MX}) or the high-frequency inflection point (f_{hIP}) of the characteristic shape of response spectra. The sensitivities with respect to Q_0 have very small values at short distances where path effects are negligible (Fig. 3). As distance increases, the effect of Q becomes more important, in contrast to the influence of the other parameters (κ_0, M_w, $\Delta\sigma$). The sensitivities due to Q_0 display a peak in the high-frequency range of the response spectrum. Consequently, the shape of the response spectrum is altered for high oscillator frequencies by slight changes in Q_0. The WNA model shows larger sensitivities with respect to Q_0 than ENA. The position of the peak of the sensitivity function with respect to Q_0 shifts to smaller f_{osc} with distance. This can be explained by the fact that high-frequency content of the input ground motion is diminished with increasing distance due to the path-related attenuation described by the quality factor $Q(f)$. Indeed, these peaks appear in different positions for WNA and ENA due to different Q_0 base values.

The sensitivities to the source-related parameters like the stress parameter ($\Delta\sigma$) and magnitude (M_w) have a relatively flat behavior (that is almost independent of f_{osc}) for values of f_{osc} above the source corner frequency f_c of the input FAS (Figs. 3 and 4). However, these sensitivity functions display a sharp increase and decrease close to f_c. The results indicate that M_w is the main influencing parameter (Fig. 4). The stress parameter $\Delta\sigma$ mainly, but not exclusively, affects the response spectral amplitudes at oscillator frequencies larger than f_c. The level of this relatively constant effect of $\Delta\sigma$ for $f_{osc} > f_c$ is stronger for WNA than for ENA, considering the same absolute change in $\Delta\sigma$ (Fig. 3). In contrast, no regional difference can be observed for M_w in Figures 3 or 4. The constant influence of M_w for large f_{osc} is approximately the same for both models and depends only slightly on M_w at small distances. However, the sensitivities with respect to M_w increase slightly with distance. The influence of M_w and $\Delta\sigma$ on response spectral amplitudes for low oscillator frequencies is explained by the fact that M_w and $\Delta\sigma$ define the source corner frequency f_c of input ground motion. For both regional models, we observe that parameters controlling the high-signal frequency content of the input FAS (κ_0, Q_0) alter the characteristic shape of response spectral amplitudes in terms of f_{MX} and f_{hIP} for large oscillator frequencies. However, M_w and $\Delta\sigma$ have a constant effect in this part of the response spectrum independent of f_{osc}. Thus, M_w and $\Delta\sigma$ only slightly affect the position of the critical points (f_{hIP}, f_{MX}), which determine the characteristic overall shape of the response spectrum for high oscillator frequencies. The influence of relative changes (relative errors) of the different inputs can be compared based on Figure 4. The impact of the same relative change is quite similar for WNA and ENA regarding M_w and $\Delta\sigma$, whereas Q_0 and κ_0 show a strong regional dependence in their relative sensitivities.

Observing the partial derivative $\partial y_{max}/\partial\kappa_0$, we see the maximum effect of κ_0 occurs in the vicinity of the f_{hIP} of the response spectrum (Fig. 5). For high κ_0 values they even coincide. Figure 5 shows the position (f_{osc}) of the maximum of $\partial y_{max}/\partial\kappa_0$ for different κ_0 together with the variation of f_{hIP} andf_{MX} with κ_0 at $R_{hypo} = 10$ km for different M_w ($5 \le M_w \le 8.5$). Indeed, for moderate-to-large earthquakes ($M_w \ge 5$) and small distances (e.g., $R = 10$ km) where path effects can be assumed negligible, κ_0 correlates strongly with the f_{hIP} and f_{MX} as depicted in Figure 5. This effect is almost independent of magnitude for large events. The frequency bandwidth between these two critical points (f_{MX}, f_{hIP}) decreases with increasing κ_0 values. Thus, in addition to these observations, the position of f_{hIP} and of f_{MX} can be used as a rough proxy to estimate κ_0 at near-source distances for large events. An estimation of the linear trends in log–log space between κ_0 and f_{MX} or f_{hIP} for WNA and ENA is given in Figure 5. This analysis is based on a simulated data set for WNA and ENA for M_w between 5 and 8.5 and different κ_0 values ranging from 0.001 to 0.1, respectively. These relations, fitted at 10 km, hold up to approximately 25 km for ENA and 23 km for WNA, allowing an error of 20% for the estimation of κ_0. For greater distances, however, the high-frequency content of the input signal is also controlled by the quality factor. As a consequence, the positions of f_{hIP} and f_{MX} are related to t^* ($t^* = \kappa_0 + R/(Q \times c_q)$) rather than to κ_0.

Sensitivities for Adjustment Issues of GMPEs

Stochastic ground-motion simulations are often applied for addressing adjustment issues of GMPEs for regions where the paucity of strong-motion data ($M_w > 5$) does not allow one to develop a reliable and indigenous GMPE. A popular framework to address this issue is the hybrid empirical approach (HEA) of Campbell (2003), which adjusts a GMPE of a host region to the region of interest (target region). To account for differences in seismological attributes, an adjustment factor $\Psi = y_{max,target}/y_{max,host}$ is applied, which is derived through stochastic ground-motion simulations. From an AD viewpoint, there are approximately 15–20 inputs (i.e., independent variables) for the regional models considered in the following example. The inputs map to a single scalar output Ψ (i.e., dependent variable) for each considered oscillator frequency.

For example, in seismic-hazard studies using the HEA, it is a common practice to calculate the adjustment factor Ψ for a single PSHA-relevant magnitude–distance scenario and apply this factor to all scenarios considered later in the seismic-hazard analysis. This procedure does not take into account the possible dependency of Ψ with respect to input variables

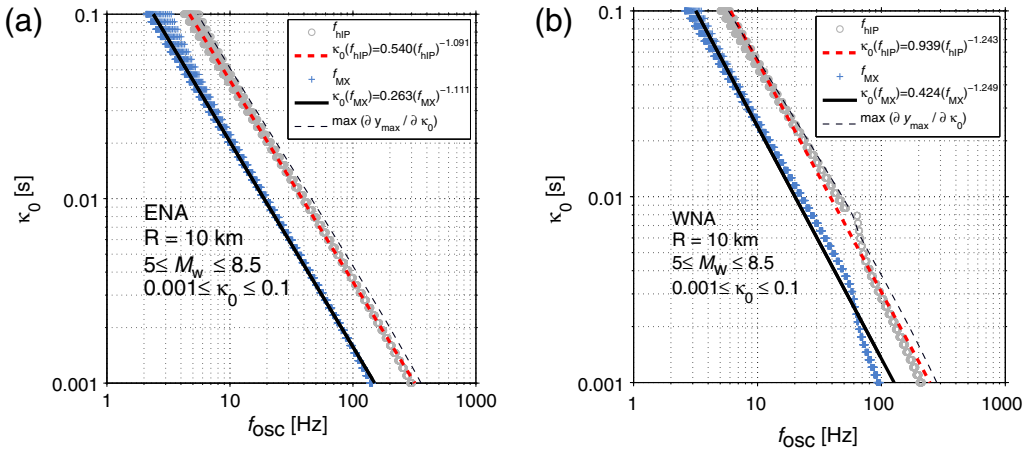

Figure 5. Variation in the position of f_{hIP} and f_{MX} with κ_0 for magnitudes $5 \le M_{\mathrm{w}} \le 8.5$ for (left) ENA and (right) WNA at $R = 10$ km. Maximum of $\partial y_{\max}/\partial \kappa_0$ is given by thin dashed lines, and trends for f_{hIP} (bold dashed lines) and f_{MX} (bold solid lines). The color version of this figure is available only in the electronic edition.

like distance and magnitude. Figure 6 shows the sensitivities of the adjustment factor Ψ for a reference scenario of M_{w} 6 and $R = 20$ km. In this example, WNA and ENA are considered as the host and target regions, respectively. See Table 5 for regional input parameter definition.

The partial derivatives of Ψ with respect to magnitude ($\partial\Psi/\partial M$) and distance ($\partial\Psi/\partial R$) do not vanish for all frequencies, as indicated in Figure 6 (second row). Thus, the adjustment factor is magnitude and distance dependent. In the example shown, an increase in earthquake magnitude of $+0.5$ results in an increase of about 10% in Ψ for frequencies in the range close to f_{c} around 0.2–0.5 Hz and a decrease for high f_{osc} (>30 Hz) of about 2%–3% in Ψ. An increase in R of $+20$ km results in an increase of Ψ of about 10%–20% for f_{osc} in the range of $2 < f_{\mathrm{osc}} < 25$ Hz, whereas Ψ decreases by a factor of 5%–10% for f_{osc} in range of 50–130 Hz. For low frequencies ($f_{\mathrm{osc}} < 1$ Hz), the adjustment factor Ψ increases by about 5%.

As a consequence, an adjustment factor derived from a single scenario could be misleading if the hazard disaggregation results in the identification of multiple relevant scenarios. Hence, in particular cases, it is reasonable to analyze these dependencies in more detail. Those estimated sensitivities are local approximations, tied to the chosen magnitude–distance scenarios, and they will probably change if the scenario is changed.

Furthermore, sensitivities of Ψ with respect to seismological host and target parameters can be very different. Thus, the effect of the parameter-associated uncertainties on the adjustment factor can strongly differ. In the example depicted in Figure 6, the last row shows the relative sensitivities of Ψ with respect to host and target κ_0 and α. These parameters control the high-frequency content of the FAS of ground motion, see equations (11) and (10) for κ_0 and α, respectively. It can be easily seen that the effect of variations in the host and target parameters on the adjustment factor is very different. For example, an uncertainty of 10% associated with host κ_0 can be approximately related to an uncertainty in Ψ of $\pm5\%$ to $\pm14\%$ for oscillator frequencies greater than 4 Hz. A similar uncertainty in target κ_0 leads to an uncertainty in Ψ of $\pm5\%$ to $\pm10\%$ for oscillator frequencies greater than 30 Hz (Fig. 6). A 10% uncertainty in host α can be approximately related to an uncertainty in Ψ of $\pm3\%$ to $\pm4.9\%$ for oscillator frequencies in the range of $8 < f_{\mathrm{osc}} < 35$ Hz (Fig. 6). However, a similar uncertainty in target α Ψ of about $\pm3\%$ to $\pm5.7\%$ for $f_{\mathrm{osc}} > 30$ Hz.

The different impact of host and target parameters on the adjustment factor can be easily estimated by the ADM and are relevant for particular earthquake scenarios in the disaggregation of seismic hazard. In particular, sensitivities can show which parameters matter most and should be addressed with a full assessment of their uncertainty.

Conclusions

The characterization of response spectral amplitude variations due to changes in seismological parameters is important for seismic-hazard analysis. In this study, we constructed an ADM using AD, which gives precise quantitative estimates of these variations (sensitivities) in an efficient way. The adjoint code was developed based on SMSIM, a proven and extensively applied simulation program for response spectra using the AD tool TAPENADE. To the best of our knowledge, this is the first time that AD has been explored in the context of seismic-hazard analysis, and its feasibility and power have been demonstrated using different sensitivity analysis examples.

The AD-based sensitivity study identified those seismological parameters that mostly influence the characteristic shape of acceleration response spectra in terms of the position of their maximum and high-frequency inflection point. The analysis was done for moderate-to-large earthquakes of engineering significance. Our results identify the parameter κ_0 as a critical parameter when using the stochastic method to

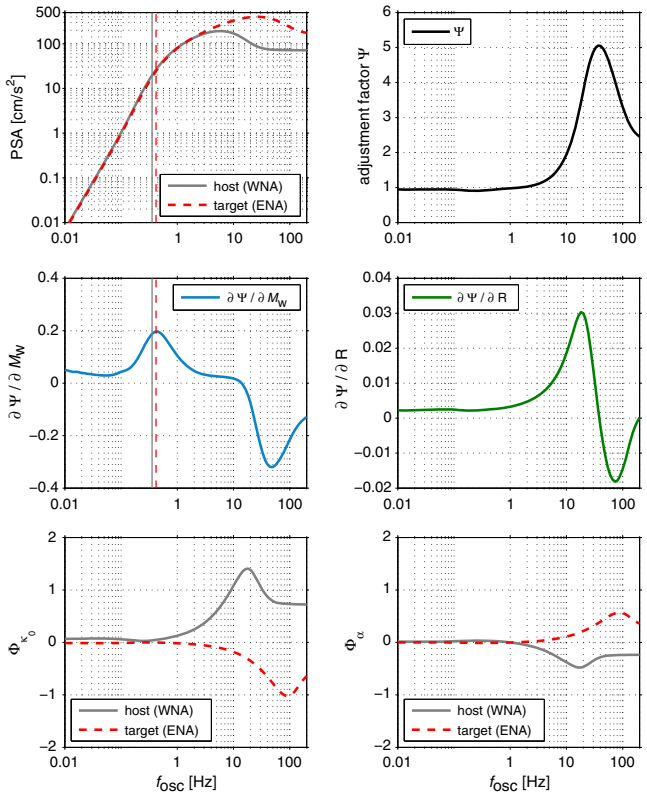

Figure 6. (First row) Simulated response spectra (left) for the host (WNA) and target region (ENA) corresponding to scenario M_w 6 and $R = 20$ km, the adjustment factor Ψ (right). (Second row) Partial derivatives of Ψ with respect to (left) M_w and (right) R. (Third row) Relative sensitivities Φ_i of Ψ with respect to (left) κ_0 and (right) α for host (WNA) and target region (ENA). The vertical lines indicate the position of source corner frequencies of the input ground motion (f_c), solid line for WNA, and dashed for ENA. The color version of this figure is available only in the electronic edition.

generate response spectral amplitudes for high oscillator frequencies at short distances. This implies the need for a better understanding of the physical origins of κ_0.

Regarding adjustment issues of GMPEs, it was shown that adjustment factors developed using the HEA depend upon magnitude and distance. This fact can be of importance in particular situations if the disaggregation of the seismic hazard suggests that multiple magnitude and distance scenarios make significant contributions to the hazard at a given return period. The use of adjustment factors that have been derived from the consideration of a single or even a small number of earthquake scenarios in seismic-hazard studies may not be justified in such cases. Uncertainties in seismological parameters can affect the adjustment in very different ways, and the AD-based ADM is a helpful tool to assess these uncertainties.

However, one has to keep in mind that the DSA is a local method. Indeed, our analyses give an estimate of first-order effects, and results may not be valid for situations far from the base case. That said, the efficiency of the approach dictates that it is not computationally expensive to consider multiple-base cases.

In the present work, we showed how a sensitivity analysis of ground-motion simulation models using the stochastic method can be carried out with the help of AD. AD delivers the otherwise unattainable derivatives of complex models, which holds great potential for other applications. For instance, we are currently working on using the ADM in optimization codes for estimating parameters of the stochastic method and their associated uncertainty. Another ongoing effort is the sensitivity analysis of hazard curves: PSHA may be viewed as a framework composed of modules with ground-motion prediction being the most critical one. Generally speaking, AD is capable of calculating the sensitivities of modules separately and combining them via the chain rule to obtain sensitivities for the entire system. Knowledge of the sensitivities of ground-motion prediction is therefore a prerequisite toward obtaining the sensitivities of a complete PSHA. We plan to couple AD with the PSHA framework to develop a sensitivity tool that would be of great value to the fields of engineering seismology and earthquake engineering.

Data and Resources

Ground-motion simulations are based on a modified version of the FORTRAN source code SMSIM provided by David Boore http://www.daveboore.com/software_online.html (last accessed December 2013). The AD tool TAPENADE http://www-sop.inria.fr/tropics/ (last accessed December 2013) is used for the algorithmic differentiation. A thorough overview of AD tools and AD methodology is given at http://www.autodiff.org (last accessed December 2013).

Acknowledgments

Christian Molkenthin is a fellow of Helmholtz graduate research school GeoSim and wishes to thank GeoSim for providing a scholarship. The authors are very grateful to Sebastian Reich, Nikos Gianniotis, Sanjay S. Bora, Annabel Händel, Hernan Leövey, and Antonia Runge for their valuable suggestions, which led to improvements of the manuscript. The authors thank Malcom Sambridge and Christine Goulet as well as Associate Editor John Douglas for many valuable comments and a thorough review that greatly improved the manuscript.

References

Anderson, J. G., and S. E. Hough (1984). A model for the shape of the Fourier amplitude spectrum of acceleration at high frequencies, *Bull. Seismol. Soc. Am.* **96,** 1969–1993.

Atkinson, G. M., and D. M. Boore (2006). Earthquake ground-motion prediction equations for eastern North America, *Bull. Seismol. Soc. Am.* **96,** 2181–2205.

Bommer, J. J., and N. A. Abrahamson (2006). Why do modern probabilistic seismic-hazard analyses often lead to increased hazard estimates? *Bull. Seismol. Soc. Am.* **96,** 1967–1977.

Boore, D. M. (1983). Stochastic simulation of high-frequency ground motions based on seismological models of the radiated spectra, *Bull. Seismol. Soc. Am.* **73,** 1865–1894.

Boore, D. M. (2003). Simulation of ground motion using the stochastic method, *Pure Appl. Geophys.* **160,** 635–676.

Boore, D. M., and W. B. Joyner (1984). A note on the use of random vibration theory to predict peak amplitudes of transient signals, *Bull. Seismol. Soc. Am.* **74,** 2035–2039.

Boore, D. M., and W. B. Joyner (1997). Site amplifications for generic rock sites, *Bull. Seismol. Soc. Am.* **87,** 327–341.

Boore, D. M., and E. M. Thompson (2012). Empirical improvements for estimating earthquake response spectra with random-vibration theory, *Bull. Seismol. Soc. Am.* **102,** 761–772.

Brune, J. N. (1970). Tectonic stress and the spectra of seismic shear waves from earthquakes, *J. Geophys. Res.* **75,** 4997–5009.

Brune, J. N. (1971). Correction to "Tectonic stress and the spectra, of seismic shear waves from earthquakes", *J. Geophys. Res.* **76,** 5002.

Campbell, K. W. (2003). Prediction of strong ground motion using the hybrid empirical method and its use in the development of ground-motion (attenuation) relations in eastern North America, *Bull. Seismol. Soc. Am.* **93,** 1012–1033.

Cartwright, D. E., and M. S. Longuet-Higgins (1956). The statistical distribution of the maxima of a random function, *Proc. Math. Phys. Sci.* **237,** 212–232.

Cotton, F., F. Scherbaum, J. J. Bommer, and H. Bungum (2006). Criteria for selecting and adjusting ground-motion models for specific target regions: Application to central Europe and rock sites, *J. Seismol.* **10,** 137–156.

Douglas, J., and P. Jousset (2011). Modeling the difference in ground-motion magnitude-scaling in small and large earthquakes, *Seismol. Res. Lett.* **82,** 504–508.

Edwards, B., and D. Fah (2013). A stochastic ground-motion model for Switzerland, *Bull. Seismol. Soc. Am.* **103,** 78–98.

Frank, P. (1978). *Introduction to System Sensitivity Theory*, Academic Press, New York, New York, 386 pp.

Gauger, N. R., A. Walther, C. Moldenhauer, and M. Widhalm (2008). Automatic differentiation of an entire design chain for aerodynamic shape optimization, in *New Results in Numerical and Experimental Fluid Mechanics VI*, Springer Berlin Heidelberg, Berlin, Germany, 454–461.

Griewank, A., and A. Walther (2008). *Evaluating Derivatives: Principles and Techniques of Algorithmic Differentiation*, Second Ed., Siam, Philadelphia, 438 pp.

Griewank, A., K. Kulshreshtha, and A. Walther (2012). On the numerical stability of algorithmic differentiation, *Computing* **94,** 125–149.

Hanks, T. C., and H. Kanamori (1979). A moment magnitude scale, *J. Geophys. Res.* **84,** 2348.

Hascoët, L., and V. Pascual (2004). TAPENADE 2.1 user's guide, *Technical Report, No. 0300*, Institut National de Recherche en Informatique et en Automatique (INRIA), Sophia Antipolis, 78 pp.

Helton, J. C. (1993). Uncertainty and sensitivity analysis techniques for use in performance assessment for radioactive waste disposal, *Reliab. Eng. Syst. Saf.* **42,** 327–367.

Ktenidou, O.-J., F. Cotton, N. A. Abrahamson, and J. G. Anderson (2014). Taxonomy of kappa: A review of definitions and estimation approaches targeted to applications, *Seismol. Res. Lett.* **85,** 135–146.

Liu, L., and S. Pezeshk (1999). An improvement on the estimation of pseudoresponse spectral velocity using RVT method, *Bull. Seismol. Soc. Am.* **89,** 1384–1389.

Marotzke, J., and R. Giering (1999). Construction of the adjoint MIT ocean general circulation model and application to Atlantic heat transport sensitivity, *J. Geophys. Res. Oceans (1978–2012)* **104,** 29,529–29,547.

Morgan, M. (1990). *Uncertainty: A Guide to Dealing with Uncertainty in Quantitative Risk and Policy Analysis*, Cambridge University Press, Cambridge, United Kingdom, 332 pp.

Naumann, U. (2012). *The Art of Differentiating Computer Programs: An Introduction to Algorithmic Differentiation*, Siam, Philadelphia, 333 pp.

Rice, S. O. (1944). Mathematical analysis of random noise, *Bell Syst. Tech. J.* **23,** 282–332.

Saltelli, A. (2000). What is sensitivity analysis? in *Sensitivity Analysis*, A. Saltelli, K. Chan, and E. M. Scott (Editors), Wiley, New York, New York, 1–12.

Sambridge, M., P. Rickwood, N. Rawlinson, and S. Sommacal (2007). Automatic differentiation in geophysical inverse problems, *Geophys. J. Int.* **170,** 1–8.

Silva, W., N. Abrahamson, G. Toro, and C. Costantino (1997). Description and validation of the stochastic ground motion model, *Final Report*, Brookhaven National Laboratory, Associated Universities, Inc., Upton, New York.

Toro, G. R. (2006). The effects of ground-motion uncertainty on seismic hazard results: Examples and approximate results, in *Annual Meeting of the Seismological Society of America*, San Francisco, California, 18–22 April 2006.

Institute of Earth & Environmental Science
University of Potsdam
Karl-Liebknecht-Str. 24-25
14476 Potsdam, Germany
molkenthin@geo.uni-potsdam.de
fs@geo.uni-potsdam.de
(C.M., F.S.)

Department of Mathematics
Humboldt-University Berlin
Unter den Linden 6
10099 Berlin, Germany
griewank@mathematik.hu-berlin.de
(A.G.)

Pacific Earthquake Engineering Research Center
325 Davis Hall
University of California
Berkeley, California 94720-1792
kuehn@berkeley.edu
(N.K.)

Department of Civil and Environmental Engineering
Imperial College London
South Kensington Campus
London SW7 2AZ, UK
p.stafford@imperial.ac.uk
(P.S.)

Manuscript received 17 January 2014;
Published Online 26 August 2014